Image reconstruction for ion imaging with the TIGRE software framework

S. Kaser[1], T. Bergauer[1], W. Birkfellner[2], D. Georg[3,4], S. Hatamikia[2,5], A. Hirtl[6], C. Irmler[1], F. Pitters[1], and F. Ulrich-Pur[1]

[1]Institute of High Energy Physics, Austrian Academy of Sciences, Vienna, Austria
[2]Center for Medical Physics and Biomedical Engineering, Medical University of Vienna, Vienna, Austria
[3]Department of Radiation Oncology, Div. Medical Radiation Physics, Medical University of Vienna, Vienna, Austria
[4]MedAustron Ion Therapy Center, Wiener Neustadt, Austria
[5]Austrian Center for Medical Innovation and Technology, Wiener Neustadt, Austria
[6]Atominstitut, TU Wien, Vienna, Austria

Abstract For ion therapy, an accurate estimate of the ion energy deposition per path length (stopping power) in the patient is essential. Ion computed tomography (iCT) allows to directly measure this quantity. However, as a result of multiple Coulomb scattering, ions pass through the patient on a curved trajectory. Considering each ion path separately in the reconstruction process adds complexity to the problem and often results in long reconstruction times. In this work, a simple and fast approach for iCT reconstruction with the GPU-based open-source software toolkit TIGRE is presented. Since the framework was initially intended for x-ray CT, a straight line approach is used to approximate ion paths to use the framework without modification.
With this simplified approach, imaging data obtained from Monte Carlo simulations and measurement data from an ion CT demonstrator are reconstructed in TIGRE. The accuracy of the demonstrated reconstruction approach is limited by the straight line approximation of the ion path. However, reconstruction results could be improved with additional data cuts. The structure of TIGRE and possibilities for its improvement for iCT reconstruction are discussed.

1 Introduction

Proton computed tomography (pCT) was already discussed by Cormack [1] in the 1960ies. Since protons and other ions are affected by multiple Coulomb scattering, they do not pass through a material on a straight line which leads to reduced image quality. An accurate path estimate is therefore necessary in the reconstruction process. Here, most likely path [2, 3] and cubic spline [4] have been shown to achieve better results than a straight line approach [5]. Although the reconstruction problem is more complex than conventional CT, ion CT (iCT) gained interest in the context of ion therapy for cancer treatment [6, 7] where treatment planning is based on the relative stopping power (RSP) values within a patient. So far, a treatment plan is based on conventional CT, where Hounsfield units (HU) have to be converted to RSP via a calibration curve [8] which is the main source of range uncertainties [9]. In iCT, the RSP can be directly obtained from the measurement, thus offering the potential for improved treatment planning in ion therapy.
A typical iCT setup, as it is displayed in Figure 1, was introduced by Schulte, Bashkirov, Li, et al. [10] and consists of a particle tracker and a device to measure the residual energy of each particle (calorimeter). The information from the tracking system is used to reconstruct the ion's path through the medium, while the residual energy is used to calculate the projection value which is then back projected along the path estimate in the reconstruction.

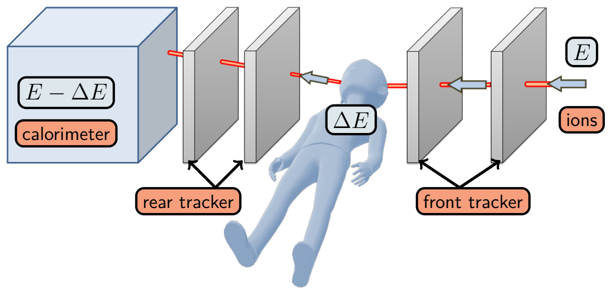

Figure 1: iCT setup consisting of two trackers, to measure the ion's position and direction and a calorimeter to measure the ion's residual energy.

Although there have already been promising ion CT reconstruction approaches [11, 12] and frameworks [13, 14], iCT reconstruction often faces problems such as long reconstruction times. The aim of the present study is to demonstrate iCT image reconstruction with the open-source framework TIGRE [15] (Tomographic Iterative GPU-based REconstruction toolbox). The layered structure of the framework allows for an iCT reconstruction approach which is fast (GPU-based reconstruction) and easy to apply for the user (Matlab user layer). Although the framework was originally intended for X-ray CT reconstruction, iCT reconstruction along straight ion paths was demonstrated to be possible.

2 Materials and Methods

2.1 TIGRE reconstruction toolkit

TIGRE is an open source cone beam CT reconstruction framework. It introduces a large set of iterative reconstruction methods, mainly algorithms using total variation (TV) regularization, which allow efficient reconstruction from sparse view and limited angle projection data. While the forward and backward projectors are fully implemented in CUDA (hence run on one or multiple GPUs), the reconstruction algorithms and user layer are written in Matlab. These layers are communicating via C++ scripts.

2.2 Ion CT demonstrator and Monte Carlo simulations

An ion CT demonstrator, consisting of four silicon strip tracking detectors and a range telescope, has been tested at MedAustron and yielded first RSP images of a phantom [16, 17]. Due to the limited size of the tracking detectors, only small phantoms can be imaged. 80 non-equidistant projections of an aluminum cube with a side length of 1 cm and a stair profile were measured over a range of 360 degrees using protons with an initial energy of 100.4 MeV.
For larger phantoms, imaging data were generated from Monte Carlo simulations with Geant4 [18] and GATE [19]. To analyze line pair resolution and RSP accuracy of the investigated reconstruction method, two Catphan modules (CTP528 and CTP404 [20]) were used as phantoms. They are made of a cylindrical acrylic body with a diameter of 15 cm and specific inserts. While the CTP528 module contains aluminum strip inserts to determine the spatial resolution of a reconstruction, the CTP404 module contains different cylindrical inserts that can be used to determine the RSP accuracy of the reconstruction (the central slice was analyzed for 200 MeV protons in [21]). In this work, reconstruction results with helium ions (200 MeV/u) are presented. Furthermore, to investigate biological materials, a CT image of the CIRS head phantom [22] was imported to a GATE simulation and a reconstruction was performed using 200 MeV protons.

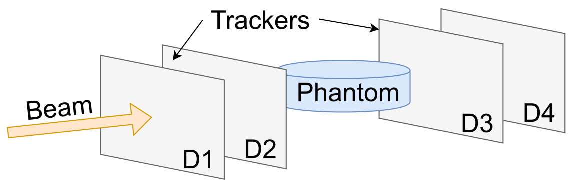

Figure 2: Monte Carlo simulation setup.

The Monte Carlo simulation setup for all simulations performed in the scope of this work (see Figure 2) consisted of two trackers, each consisting of two silicon detectors. One tracker was located upstream (detector D1 and detector D2) and one downstream (detector D3 and detector D4) the phantom to measure entry and exit position and direction of ions to the phantom. Between the two detectors of a tracker, a 10 cm distance was set while the distance between tracker and phantom was always kept greater than 10 cm. The residual energy of the ions was determined at detector D4 in this idealized setup (no additional calorimeter). The setup was located within an air volume and a fluence of 800 ions/mm^2 (Catphan modules) and 200 ions/mm^2 (CIRS head) was used in the simulations. In each simulation, 90 projections were generated over an angular span of 178°.

2.3 iCT projection definition and reconstruction

To use the framework TIGRE without modification, a straight line approach was used for the ion path. In order to remove ion paths with a strong curvature, position cuts were introduced in addition to the standard 3σ cuts [3]: The difference of proton hit positions in x- and y-direction between detector D2 and detector D3 was calculated and, if it exceeded a certain threshold, the track was rejected (this method was adapted from Cirrone, Bucciolini, Bruzzi, et al. [23]). The optimal position cut threshold hereby depended on the phantom thickness and material. It was set to 0.5 mm for the measurement data, 2 mm for the simulation of Catphan modules and 4 mm for the simulation of the CIRS head since this was found to be the ideal compromise between optimized spacial resolution, RSP accuracy and amount of rejected ion paths. If a track passed the cut condition, the ion was assigned to the pixel corresponding to the average of the hit positions on detectors D2 and D3.
To obtain the RSP in the reconstructed image, the water equivalent path length (WEPL) had to be calculated for each ion and further used as projection value. While for the measurements from the iCT demonstrator, the range telescope measurement was directly converted to the WEPL, the Donahue [24] definition of the ion range R,

$$R = \frac{1}{\kappa}[\beta E_{\text{in}}^{q} + \alpha E_{\text{in}}^{p} + \frac{h}{g}(\exp(-gE_{\text{in}}) + gE_{\text{in}} - 1)]u, \quad (1)$$

was used for simulated data. Here, the stopping power S depends on the material's ionization potential I_{material} and the ion energy E. E_{in} is the initial ion energy and u is the atomic mass number of the ion. α, β, g, h, p, and q are material-dependent parameters, which were already defined for protons in water in Donahue, Newhauser, and Ziegler [24]. For helium ions, the material parameters for the Donahue model were calibrated with NIST data [25] between 5 MeV to 250 MeV using a least squares algorithm implemented in scipy [26]. To obtain the WEPL for each ion, the range at the initial and residual ion energy E_{in} and E_{out} are subtracted [21]

$$\text{WEPL} = R_{\text{water}}(E_{\text{in}}) - R_{\text{water}}(E_{\text{out}}). \quad (2)$$

In the projection, the average WEPL per pixel was calculated for all ions assigned to the pixel.
Adaptive-Steepest-Descent Projection Onto Convex Sets (ASD-POCS) [27] of the Total Variation (TV) algorithm family was selected as the main reconstruction method in this study due to its highly demonstrated performance under limited angle scanning trajectories. Algorithms of this family have also shown promising results for iCT reconstruction problems [28, 29]. In [21] it was shown that especially for limited data, ASD-POCS outperforms other algorithms implemented in TIGRE, such as Ordered-Subset Simultaneous Algebraic Reconstruction Technique (OS-SART) [30]. However, OS-SART was used to reconstruct the measurement data from the iCT demonstrator at MedAustron. Due to the phantom size, the data cuts did not have such a strong influ-

ence and the better statistics per pixel allowed for the faster reconstruction with OS-SART.

3 Results

3.1 Measurement data from the iCT demonstrator

In the reconstructed 3D view of the phantom (Figure 3, right), the stair profile is clearly visible. Furthermore, the reconstructed RSP was analyzed within each stair (see Figure 4). Edge voxels have been excluded from this analysis. The relative error of the median RSP within each step was ranging from 1.4% to 11% (thinnest stair), while the relative error of the average values was ranging from 2.7% to 11.6%.

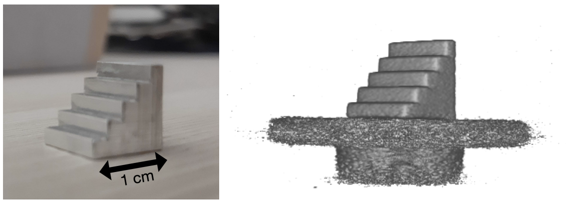

Figure 3: Photo of aluminum phantom (left) and 3D view of its reconstruction (right). 3D view was created with Slicer [31].

In Ulrich-Pur, Bergauer, Burker, et al. [17], the RSP values within the phantom stairs (again, after using position cuts of 0.5 mm) were analyzed while including edge voxels. It could be seen that the relative error of the most probable value (MPV) within a stair could be lowered to 0.28 - 1.56% with these position cuts. The reason for the smaller errors compared to the values stated before lies in the shape of the RSP distribution observed within a stair: Rather than being Gaussian-shaped, the distribution showed a significant tail towards lower values. While this influences the average and median value within a stair and shifts it to a lower value, the MPV could still be found closer to the expected reference value.

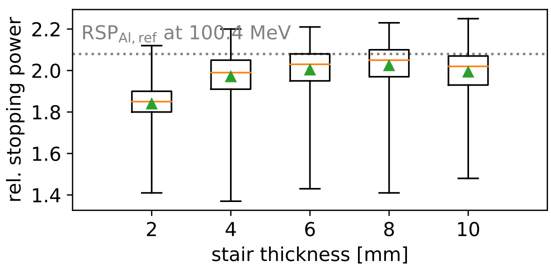

Figure 4: Reconstructed RSP values within the stairs.

3.2 Monte Carlo simulations – Catphan modules

Based on the work in Kaser, Bergauer, Birkfellner, et al. [21] reconstruction results using helium ions are summarized in Figure 5 for the central slices of the CTP528 and CTP404 modules.

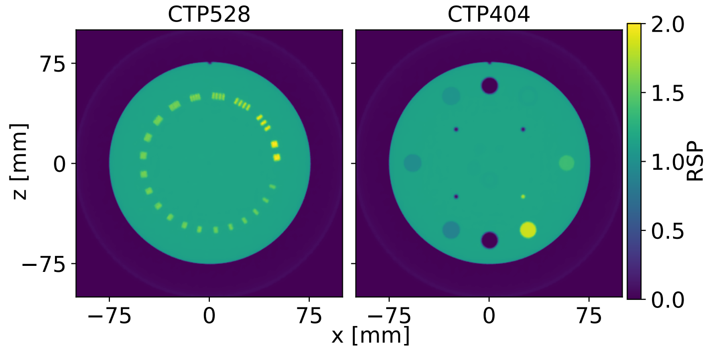

Figure 5: Reconstructed central slices of CTP528 (left) and CTP404 (right) using 200 MeV/u helium ions.

The contrast of the first three line pair inserts within the CTP528 from a reconstruction using protons or helium ions and a 2 mm position cut is shown in Figure 6. While the 3 line pair insert could be distinguished with a contrast of 26% for protons, the contrast of higher line pair inserts was below 10%. Using helium ions, the contrast for the first three line pairs was higher than for protons, for example, 40% for the 3 line pair insert.

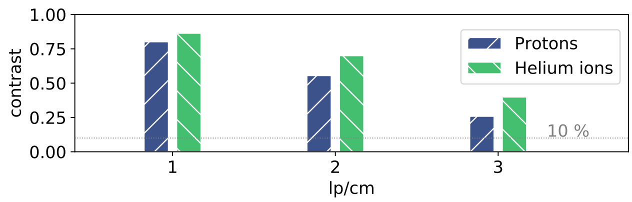

Figure 6: Contrast values in the line pair inserts of the CTP528.

For the CTP404, RSP values of three from the outer inserts, namely LDPE (Low Density Polyethylen), PMP (Polymethylpentene) and Delrin, can be found in Figure 7 for protons and helium ions. Edge pixels have been excluded from the analysis.

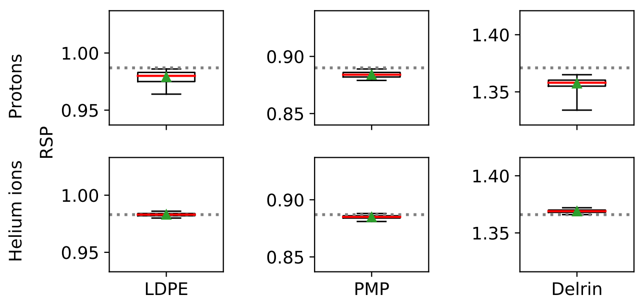

Figure 7: Reconstructed RSP values in the LDPE, PMP and Delrin insert.

For helium ions, the spread of values was smaller than for protons within a region of interest. Furthermore, the average RSP did correspond very well to the the reference RSP, which was defined using an R80 calibration. For example, the reconstructed average RSP for the Delrin insert yielded 1.369 which is 0.2% above the reference value of 1.366. For protons, the average RSP value of 1.357 was approximately 1% below the reference value (1.371).

3.3 Monte Carlo simulations – CIRS head phantom

To visually demonstrate the effect of position cuts on the reconstruction result, a CT image of the CIRS head phantom was inserted as phantom to a GATE simulation. Figure 8 shows the reconstruction result from 90 projections using 200 MeV protons.
The effect of the position cuts can be visually observed regarding the transition between bone and tissue within the phantom.

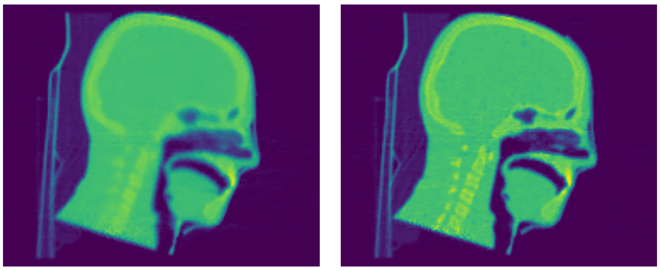

Figure 8: Reconstructed slices of CIRS head phantom without (left) and with (right) position cuts.

4 Discussion

To apply the OS-SART and the ASD-POCS algorithm (based on total variation) to the iCT reconstruction problem, no modification of the TIGRE software framework was necessary (only a redefinition of projection values).
Measurement data from an ion CT demonstrator could be successfully reconstructed and position cuts could be used to increase RSP accuracy. The reconstruction time for a volume of $256 \times 256 \times 128$ voxels was smaller than 10 s on a standard GPU using OS-SART.
For larger phantoms, Monte Carlo simulations were used to generate projection data. The reconstruction of the CTP528 using protons showed the expected limitations in spatial resolution due to the straight line approximation of the proton path. Nevertheless, inserts with 1 to 3 lp/cm could be distinguished using the additional position cut. Comparing reconstruction results to other straight line reconstructions using protons, a similar spatial resolution can be found (for example approx. 2 lp/cm for 180 projections and using ART with 120 iterations and 200 protons mm^{-2} in Li, Liang, Singanallur, et al. [5]). Using helium ions instead of protons did increase the contrast of the reconstruction result.
For the CTP404, RSP values within inserts were analyzed (transitions between materials were neglected in the analysis for this phantom). Regarding the average RSP values obtained in the inserts, the Donahue approximation seems to be an adequate option for the projection definition since only minor deviations from the literature values [32] were found.
For helium ions, reconstructed RSP values were closer to the reference value than for proton ions.
For the CIRS head phantom, the effect of position cuts could be well observed regarding the transitions between phantom/air and bone/tissue in Figure 8.
To further test the applicability of TIGRE for limited projection data, the number of projections or the particle fluence used in this study have to be further reduced. However, the 800 protons/mm^2 that were used in the present work lie in the typical range for iCT: For example, Rit, Dedes, Freud, et al. [11] used 900 protons per mm^2 to investigate a 3 lp/cm insert (720 projections) while Giacometti, Bashkirov, Piersimoni, et al. [33] reported a contrast above 10 % for 3 lp/cm for 100 protons per mm^2 and 90 projections.
The main limitations of the presented method arise from the effect of multiple Coulomb scattering, which leads to decreased spatial resolution and RSP inaccuracies if a straight ion path is assumed. The position cut used in the present study allowed to compensate for this effect to some part, however, a large number of primary particles were filtered (70-90%). Using helium ions, 34-75% of primary ions were rejected by the 2 mm position cut. To optimize TIGRE for iCT, two main requirements have to be addressed: The already binned projection data have to be replaced by list-mode data. This step is crucial to treat each ion path separately in the reconstruction process. Here, the straight line approximation has to be replaced by cubic spline or most likely path estimation.
The structure of TIGRE allows to keep a Matlab header for the user while changes in the projection and back projection operators have to be done in CUDA. Such changes in the CUDA implementations have already been proposed in Hatamikia, Biguri, Kronreif, et al. [34], where reconstruction from arbitrary rotation scan trajectories were added to the framework. In addition, the CUDA layer was modified to speed up the implementation of the total-variation based algorithms. The TIGRE toolbox offers multiple incentives to perform the proposed adaptions for iCT: It offers a wide range of algorithms which have already been shown to generate promising results with low input data [15, 34], the use of multi-GPUs is possible and the layered structure makes the framework a promising candidate for a user-friendly iCT reconstruction framework. This layer structure already allows the use of multi-GPUs in the reconstruction, further speeding up the reconstruction time.

5 Conclusion

The applicability of the TIGRE reconstruction framework to the ion CT reconstruction problem was shown using simulated and measured projection data. Further improvements needed to optimize ion CT reconstruction were discussed. Most importantly, a sophisticated path estimate has to be implemented to the framework.

6 Acknowledgements

The authors would like to thank Barbara Knäusl (MedUni Wien) and Markus Stock (MedAustron) for providing the CT image of the CIRS head phantom. This project received funding from the Austrian Research Promotion Agency (FFG), grant number 875854.

References

[1] A. M. Cormack. "Representation of a function by its line integrals, with some radiological applications". *Journal of Applied Physics* 34.9 (1963), pp. 2722–2727. DOI: 10.1063/1.1729798.

[2] D. Williams. "The most likely path of an energetic charged particle through a uniform medium". *Physics in Medicine & Biology* 49.13 (2004), p. 2899. DOI: 10.1088/0031-9155/49/13/010.

[3] R. Schulte, S. Penfold, J. Tafas, et al. "A maximum likelihood proton path formalism for application in proton computed tomography". *Medical Physics* 35.11 (2008), pp. 4849–4856. DOI: 10.1118/1.2986139.

[4] C.-A. C. Fekete, P. Doolan, M. F. Dias, et al. "Developing a phenomenological model of the proton trajectory within a heterogeneous medium required for proton imaging". *Physics in Medicine & Biology* 60.13 (2015), p. 5071. DOI: 10.1088/0031-9155/60/13/5071.

[5] T. Li, Z. Liang, J. V. Singanallur, et al. "Reconstruction for proton computed tomography by tracing proton trajectories: A Monte Carlo study". *Medical physics* 33.3 (2006), pp. 699–706. DOI: 10.1118/1.2171507.

[6] R. Schulte, V. Bashkirov, T. Li, et al. "Conceptual design of a proton computed tomography system for applications in proton radiation therapy". *IEEE Transactions on Nuclear Science* 51.3 (2004), pp. 866–872. DOI: 10.1109/TNS.2004.829392.

[7] U. Schneider, J. Besserer, P. Pemler, et al. "First proton radiography of an animal patient". *Medical Physics* 31.5 (2004), pp. 1046–1051. DOI: 10.1118/1.1690713.

[8] U. Schneider, E. Pedroni, and A. Lomax. "The calibration of CT Hounsfield units for radiotherapy treatment planning". *Physics in Medicine and Biology* 41.1 (1996), pp. 111–124. DOI: 10.1088/0031-9155/41/1/009.

[9] M. Yang, X. R. Zhu, P. C. Park, et al. "Comprehensive analysis of proton range uncertainties related to patient stopping-power-ratio estimation using the stoichiometric calibration". *Physics in Medicine & Biology* 57.13 (2012), p. 4095. DOI: 10.1088/0031-9155/57/13/4095.

[10] R. W. Schulte, V Bashkirov, T. Li, et al. "Conceptual design of a proton computed tomography system for applications in proton radiation therapy". *IEEE Transactions on Nuclear Science* 51.3 (2004), pp. 866–872. DOI: 10.1109/TNS.2004.829392.

[11] S. Rit, G. Dedes, N. Freud, et al. "Filtered backprojection proton CT reconstruction along most likely paths". *Medical Physics* 40.3 (2013), p. 031103. DOI: 10.1118/1.4789589.

[12] D. C. Hansen, T. S. Sørensen, and S. Rit. "Fast reconstruction of low dose proton CT by sinogram interpolation". *Physics in Medicine & Biology* 61.15 (2016), p. 5868. DOI: 10.1088/0031-9155/61/15/5868.

[13] M. S. Hansen and T. S. Sørensen. "Gadgetron: an open source framework for medical image reconstruction". *Magnetic Resonance in Medicine* 69.6 (2013), pp. 1768–1776. DOI: 10.1002/mrm.24389.

[14] P. Karbasi, R. Cai, B. Schultze, et al. "A highly accelerated parallel multi-gpu based reconstruction algorithm for generating accurate relative stopping powers". *2017 IEEE Nuclear Science Symposium and Medical Imaging Conference (NSS/MIC)*. IEEE. 2017, pp. 1–4. DOI: 10.1109/NSSMIC.2017.8532871.

[15] A. Biguri, M. Dosanjh, S. Hancock, et al. "TIGRE: a MATLAB-GPU toolbox for CBCT image reconstruction". *Biomedical Physics & Engineering Express* 2.5 (2016), p. 055010. DOI: 10.1088/2057-1976/2/5/055010.

[16] F. Ulrich-Pur, T. Bergauer, A. Burker, et al. "Imaging with protons at MedAustron". *Nuclear Instruments and Methods in Physics Research Section A: Accelerators, Spectrometers, Detectors and Associated Equipment* (2020), p. 164407. DOI: 10.1016/j.nima.2020.164407.

[17] F. Ulrich-Pur, T. Bergauer, A. Burker, et al. *A Proton Computed Tomography Demonstrator for Stopping Power Measurements*. 2021. URL: https://arxiv.org/abs/2106.12890.

[18] S. Agostinelli, J. Allison, K. a. Amako, et al. "GEANT4—a simulation toolkit". *Nuclear instruments and methods in physics research section A: Accelerators, Spectrometers, Detectors and Associated Equipment* 506.3 (2003), pp. 250–303. DOI: 10.1016/S0168-9002(03)01368-8.

[19] D. Strulab, G. Santin, D. Lazaro, et al. "GATE (Geant4 Application for Tomographic Emission): a PET/SPECT general-purpose simulation platform". *Nuclear Physics B-Proceedings Supplements* 125 (2003), pp. 75–79. DOI: 10.1016/S0920-5632(03)90969-8.

[20] The Phantom Laboratory. *Catphan 600® Manual*. Accessed: 2021-01-15. 2015. URL: https://www.phantomlab.com/catphan-600.

[21] S. Kaser, T. Bergauer, W. Birkfellner, et al. "First application of the GPU-based software framework TIGRE for proton CT image reconstruction". *Physica Medica* 84 (2021), pp. 56–64. DOI: 10.1016/j.ejmp.2021.03.006.

[22] *Phantom Patient for Stereotactic End-to-End Verification*. Accessed: 23-June-2021. URL: https://www.cirsinc.com/products/radiation-therapy/phantom-patient-for-stereotactic-end-to-end-verification/.

[23] G. A. P. Cirrone, M. Bucciolini, M. Bruzzi, et al. "Monte Carlo evaluation of the Filtered Back Projection method for image reconstruction in proton computed tomography". *Nuclear Instruments and Methods in Physics Research Section A: Accelerators, Spectrometers, Detectors and Associated Equipment* 658.1 (2011), pp. 78–83. DOI: 10.1016/j.nima.2011.05.061.

[24] W. Donahue, W. D. Newhauser, and J. F. Ziegler. "Analytical model for ion stopping power and range in the therapeutic energy interval for beams of hydrogen and heavier ions". *Physics in Medicine & Biology* 61.17 (2016), p. 6570. DOI: https://doi.org/10.1088/0031-9155/61/17/6570.

[25] M. Berger, J. Coursey, M. Zucker, et al. *Stopping-power and range tables for electrons, protons, and helium ions, NIST Standard Reference Database 124*. 2017. DOI: 10.18434/T4NC7P.

[26] P. Virtanen, R. Gommers, T. E. Oliphant, et al. "SciPy 1.0: fundamental algorithms for scientific computing in Python". *Nature methods* 17.3 (2020), pp. 261–272. DOI: 10.1038/s41592-019-0686-2.

[27] E. Y. Sidky and X. Pan. "Image reconstruction in circular cone-beam computed tomography by constrained, total-variation minimization". *Physics in Medicine & Biology* 53.17 (2008), p. 4777. DOI: 10.1088/0031-9155/53/17/021.

[28] B. Schultze, Y. Censor, P. Karbasi, et al. "An improved method of total variation superiorization applied to reconstruction in proton computed tomography". *IEEE Transactions on Medical Imaging* 39.2 (2019), pp. 294–307. DOI: 10.1109/TMI.2019.2911482.

[29] J. Lee, C. Kim, B. Min, et al. "Sparse-view proton computed tomography using modulated proton beams". *Medical physics* 42.2 (2015), pp. 1129–1137. DOI: 10.1118/1.4906133.

[30] Y. Censor et al. "Block-Iterative Algorithms with Diagonally Scaled Oblique Projections for the Linear Feasibility Problem". *SIAM Journal on Matrix Analysis and Applications* 24.1 (2002), pp. 40–58. DOI: 10.1137/S089547980138705X.

[31] S. Pieper, M. Halle, and R. Kikinis. "3D Slicer". *2004 2nd IEEE international symposium on biomedical imaging: nano to macro (IEEE Cat No. 04EX821)*. IEEE. 2004, pp. 632–635. DOI: 10.1109/ISBI.2004.1398617.

[32] J. Zhu and S. N. Penfold. "Dosimetric comparison of stopping power calibration with dual-energy CT and single-energy CT in proton therapy treatment planning". *Medical Physics* 43.6 Part 1 (2016), pp. 2845–2854. DOI: 10.1118/1.4948683.

[33] V. Giacometti, V. A. Bashkirov, P. Piersimoni, et al. "Software platform for simulation of a prototype proton CT scanner". *Medical Physics* 44.3 (2017), pp. 1002–1016. DOI: 10.1002/mp.12107.

[34] S. Hatamikia, A. Biguri, G. Kronreif, et al. "Optimization for customized trajectories in cone beam computed tomography". *Medical Physics.* (2020). DOI: 10.1002/mp.14403.